Coexisting commensurate and incommensurate magnetic orders in the double double perovskite CaMnCoWO6

Journal of Inorganic and General Chemistry
ZAAC
Zeitschrift für anorganische und allgemeine Chemie
www.zaac.wiley-vch.de
RESEARCH ARTICLE

DOI: 10.1002/zaac.202300047

Coexisting commensurate and incommensurate magnetic orders in the double double perovskite $CaMnCoWO_6$

Kunlang Ji,[a] Ruichao Chen,[a] Pascal Manuel,[b] and J. Paul Attfield*[a]

Dedicated to Antoine Maignan on his 60th Birthday.

A new double double perovskite of ideal composition $CaMnCoWO_6$ has been synthesised at high pressure. The structure is tetragonal ($P4_2/n$, $a = 7.6651(3)$, $c = 7.6822(3)$ Å) and disorder between A-site Mn^{2+} and B-site Co^{2+} leads to a Co-rich off-stoichiometric composition $CaMn_{0.8}Co_{1.2}WO_6$ [$Ca(Mn_{0.65}Co_{0.35})(Co_{0.86}Mn_{0.14})WO_6$]. An unusual combination of commensurate and incommensurate spin orders (A-site Mn/Co spins with propagation vector (0.5 0.5 0.5) and B-site Co/Mn spins with (0.5 0.42 0.5)) is observed below a magnetic transition at $T_C = 18$ K. This is the first discovery of complex magnetism in the double double perovskite family.

Introduction

Many interesting and useful oxide materials are based on the ABO_3 perovskite type,[1,2] and cation ordering can lead to further properties such as ferrimagnetism and large magnetoresistance in Sr_2FeMoO_6 and related $A_2BB'O_6$ double perovskites.[3,4,5,6,7] High pressure can be used to stabilize perovskites with the small high spin Mn^{2+} ion at A-sites,[8] for example, $MnVO_3$ which has helimagnetic order at low temperatures.[9] Mn^{2+}-based double perovskites have also been prepared at pressure; Mn_2BSbO_6 for B = Sc,[10] Cr,[11] and Fe[12] which has low temperature incommensurate Mn spin order; and the Mn_2BReO_6 series for B = Mn,[13] Fe,[14,15] Co,[16] and Ni.[17] Mn_2FeReO_6 is notable for having a high Curie temperature of 520 K and similar ferrimagnetic and spin-polarised conducting properties to Sr_2FeMoO_6, but also with a switch from negative to large positive magnetoresistances at low temperatures driven by Mn^{2+} spin ordering. The small size of the Mn^{2+} cation leads to tilting distortions in these perovskites so that $MnVO_3$ has the orthorhombic $GdFeO_3$-type perovskite structure and the Mn_2BSbO_6 materials have a monoclinically-distorted $P2_1/n$ symmetry structure.

Further research on A-site Mn^{2+} perovskites led to the discovery of a new $AA'BB'O_6$ double double perovskite type. They all have a tetragonal $P4_2/n$ structure with columnar ordering of 10-coordinate A and 4-coordinate A′ cations. A = R (rare earth) $RMnMnB'O_6$ series are reported for B′ = Sb[18,19] and Ta,[20] and many $CaMnBB'O_6$ materials (B = Mn, Fe, Co, Ni for B′ = Re,[21,22,23] and B/B′ = Fe/Ta,[24] Cr/Sb and Fe/Sb,[25] Mn/W,[26] and Fe/Nb)[27] have also been synthesised at high temperatures and pressures. Recently $P4_2/n$ double double perovskites based on A′ cations other than Mn^{2+} have been reported in $CaCuFeReO_6$[28] and $CaFeFeNbO_6$.[27]

Most of the $P4_2/n$ double double perovskite materials have simple ferri- or ferro- magnetic orders commensurate with the crystal unit cell (propagation vector $\boldsymbol{k} = (0\ 0\ 0)$), although $CaMnFeTaO_6$, $CaMnFeNbO_6$, and $CaFeFeNbO_6$ have shown spin glass ground states without long range spin ordering due to substantial cation disorder.[24,27] Two materials, $CaMnMnWO_6$ and $SmMnMnTaO_6$, were discovered to undergo thermal transformations from $AA'BB'O_6$ double double perovskite structures, where both A and B sites have 1:1 cation order, to $(A_{0.5}A'_{0.5})_2BB'O_6$ double perovskites with fully disordered A/A′ cations under pressure.[26] For $CaMnMnWO_6$ this leads to a drastic change of magnetic properties from ferrimagnetic order in the double double perovskite form to spin glass behaviour in the highly frustrated double perovskite polymorph. This motivated the present exploration of the analogue $CaMnCoWO_6$ which is discovered to form an off-stoichiometric double double perovskite $CaMn_{0.8}Co_{1.2}WO_6$ with co-existing commensurate and incommensurate spin orders, the first time that such complex magnetism has been observed in this family of materials.

Results and Discussion

Samples of ideal composition $CaMnCoWO_6$ were synthesized at 12 GPa and 1200 °C as described in the Experimental Section. Fits to the powder X-ray diffraction profile (Figure 1) showed that the majority phase is a $P4_2/n$ double double perovskite, but secondary $CaWO_4$ and (Mn,Co)O phases were present and were not eliminated in repeated syntheses. A fit

[a] Dr. K. Ji, R. Chen, Prof. J. P. Attfield
Centre for Science at Extreme Conditions (CSEC) and
School of Chemistry,University of Edinburgh
Mayfield Road, Edinburgh EH9 3JZ (UK)
E-mail: j.p.attfield@ed.ac.uk
[b] Dr. P. Manuel
STFC Rutherford Appleton Lab, ISIS Facility, Harwell Science and Innovation Campus, Didcot, OX11 0QX, UK

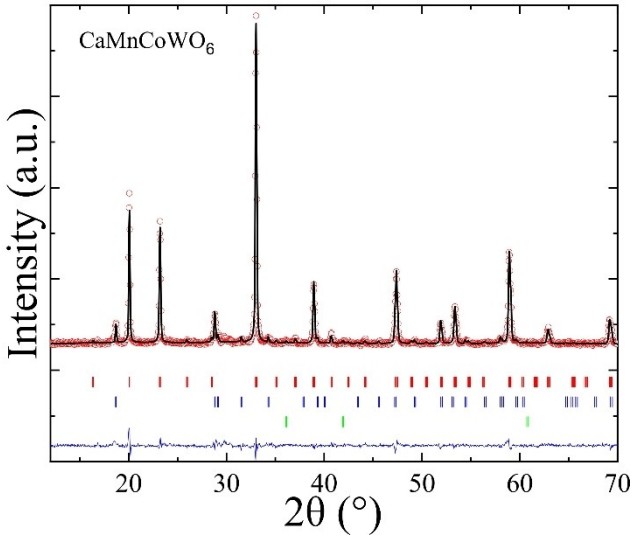

Figure 1. Rietveld fit to the room temperature powder X-ray diffraction pattern of double double perovskite $CaMnCoWO_6$ (red Bragg markers, 91.5 wt%) and $CaWO_4$ (blue markers, 7.2(2)%) and (Mn,Co)O (green markers, 1.3(2)%) impurities.

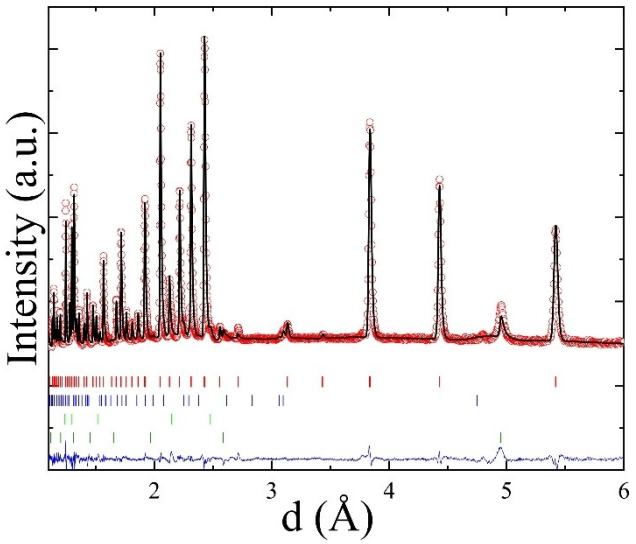

Figure 2. Rietveld fit to the powder neutron pattern of $CaMnCoWO_6$ at 150 K. Bragg markers show $CaMnCoWO_6$ (red, 96.7 wt%), $CaWO_4$ (blue, 1.6(2)%) and (Mn,Co)O nuclear (light green,1.7(1)%) and magnetic (dark green) contributions.

to high resolution time-of-flight powder neutron diffraction data collected at 150 K was used to confirm the crystal structure and analyse cation site occupancies, making use of the high Co/Mn neutron contrast ($b = 2.78/-3.73$ fm). Results are given in Table 1 and Figures 2 and 3.

Table 1. Crystal structure parameters for $CaMnCoWO_6$ from the 150 K $P4_2/n$ neutron Rietveld fit with derived bond distances below. Cell parameters are $a = 7.6651(3)$ and $c = 7.6822(3)$ Å.[a]

Atom[b]	x	y	z	B_{iso} (Å^2)
Ca	0.2500	0.7500	0.7769(5)	2.43(11)
A1(Mn/Co)	0.7500	0.7500	0.7500	1.2(2)
A2(Mn/Co)	0.2500	0.2500	0.7500	1.2
B1(Co/Mn)	0.0000	0.5000	0.5000	1.2
B2(W)	0.0000	0.0000	0.5000	1.07(9)
O1	−0.0547(8)	0.5605(8)	0.2365(6)	0.73(4)
O2	−0.2365(9)	−0.0492(3)	0.5715(2)	0.73
O3	−0.2616(9)	0.0579(3)	−0.0351(3)	0.73
Distances (Å)				
Ca–O1 (x2)		2.768(7)	B1-O1 (x2)	2.119(5)
Ca–O1 (x2)		2.814(7)	B1-O2 (x2)	2.127(7)
Ca–O2 (x2)		2.574(3)	B1-O3 (x2)	2.071(7)
Ca–O3 (x2)		2.471(4)	<B1-O>	2.106(6)
Ca–O3 (x2)		2.373(4)	B2-O1 (x2)	1.921(5)
<Ca–O>		2.600(5)	B2-O2 (x2)	1.931(7)
A1–O2 (x4)		2.064(3)	B2-O3 (x2)	1.900(7)
A2–O1 (x4)		2.088(7)	<B2-O>	1.918(6)

[a] Residuals: $R_p = 2.99\%$, $R_{wp} = 2.77\%$, $R_{Bragg} = 3.21\%$, $R_F = 4.55\%$, $\chi^2 = 3.08$. [b] Wyckoff sites; Ca 4e, A1, 2a; A2, 2b; B1, 4c; B2, 4d; O1-O3, 8g. Site occupancies; A1 Mn/Co = 0.640/0.360(12); A2 Mn/Co = 0.660/0.340(12); B1 Co/Mn = 0.864/0.136(4); other sites are fully occupied.

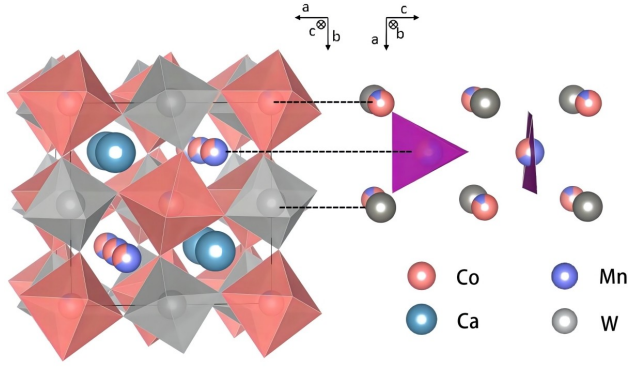

Figure 3. Crystal structure of $CaMnCoWO_6$ in space group $P4_2/n$ showing the alternating arrangement of tetrahedral and square-planar Mn^{2+} sites (part-occupied by Co^{2+}) in A′ cation columns (sites A1 and A2) at the right.

Refinement results in Table 1 show a substantial disorder within the AA′BB′O_6 double double perovskite structure between A′(Mn) and B(Co) sites, with ~35% substitution by Co at the former and 14% Mn at the latter. (There are two A′ sites, shown as A1 and A2 in Table 1, with respective tetrahedral and square planar oxide coordinations, the latter being relatively unusual for Mn^{2+} and Co^{2+}.) This disorder leads to an overall Co-rich refined composition of $CaMn_{0.79(2)}Co_{1.21(2)}WO_6$. However no interchange of W^{6+} with either Co^{2+} or Mn^{2+} is observed, reflecting the large difference in ionic charges and also the smaller size of W^{6+} which leads to B2(W)-O distances of 1.90–1.93 Å whereas Co/Mn-O distances are in the range 2.06–2.13 Å at the A1, A2, and B1 sites.

Magnetisation measurements for a $CaMnCoWO_6$ sample are shown in Figure 4. The susceptibility χ follows Curie-Weiss

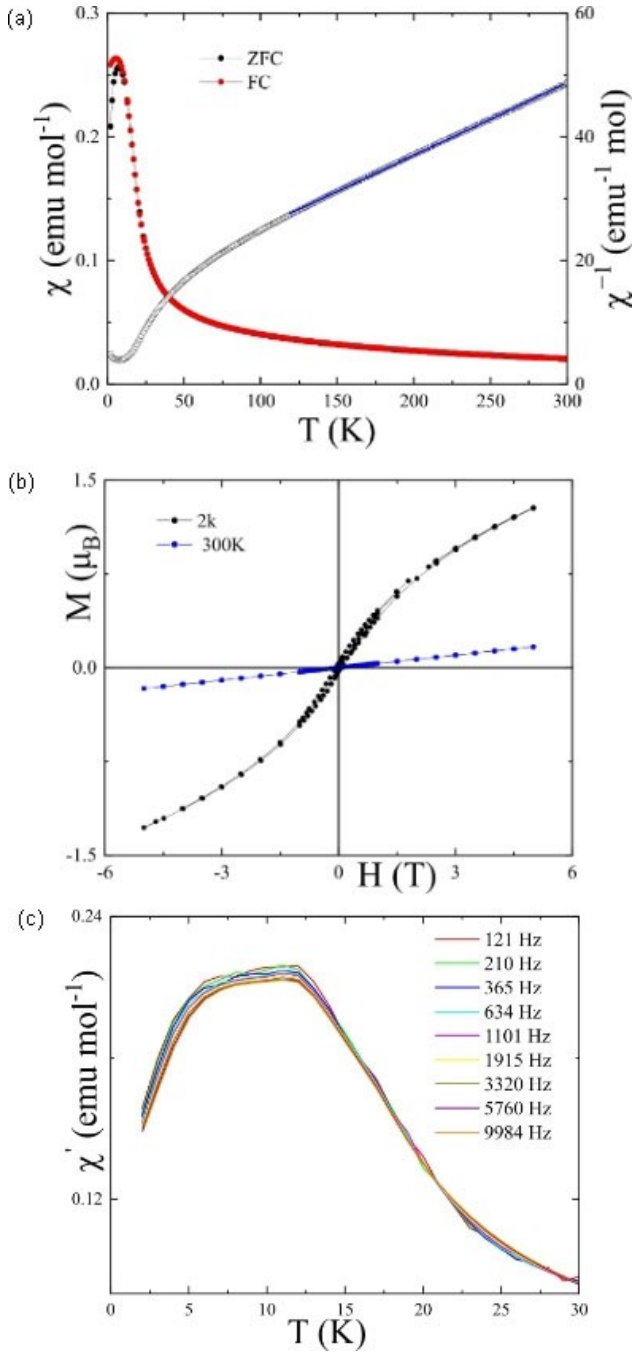

Figure 4. Magnetic measurements for $CaMnCoWO_6$. (a) ZFC and FC susceptibilities under a 0.1 T field, and the inverse susceptibility showing a Curie-Weiss fit. (b) Magnetisation-field loops at 2 and 300 K. (c) Low temperature ac susceptibility at various frequencies.

paramagnetic behavior at high temperatures and the fitted Weiss constant of $\theta = -117$ K indicates dominant antiferromagnetic spin-spin interactions. The fitted effective paramagnetic moment of 8.26(1) μ_B per $CaMnCoWO_6$ unit is larger than the theoretical spin-only value of 7.07 μ_B for high spin Co^{2+} and Mn^{2+}, most likely reflecting a substantial orbital contribution for Co^{2+} although impurity effects could also contribute. A broad susceptibility peak is observed below a transition (estimated from the maximum $-d\chi/dT$ slope) at $T_C = 18$ K with divergence of zero-field cooled (ZFC) and field-cooled (FC) susceptibilities. This and the magnetization-field loop at 2 K in Fig. 4b could be consistent with ferro/ferrimagnetism or spin glass behavior, however, the peak shows no significant frequency dependence in ac measurements in Fig. 4c which would be diagnostic of a spin-glass ground state.

Further powder neutron diffraction patterns were collected at low temperatures to investigate possible spin ordering (Figure 5). These reveal several weak magnetic peaks that disappear on warming from 15 to 20 K, consistent with the measured $T_C = 18$ K. The most intense magnetic peak is indexed by wavevector $\boldsymbol{k} = (0.5\ 0.5\ 0.5)$ but adjacent satellite reflections are indexed by incommensurate $\boldsymbol{k} = (0.5\ k_y\ 0.5)$ with $k_y \approx 0.42$. This suggests that A and B site spin orders have different propagation vectors, both based on a simple antiferromagnetic arrangement as $\boldsymbol{k} = (0.5\ 0.5\ 0.5)$ corresponds to a $2\times2\times2$ magnetic supercell, but with one possessing a further incommensurate modulation. Trial fits of magnetic models to the 1.4 K profile showed that the (0.5 0.5 0.5) order is of the A1 and A2 (Mn-rich) site spins, while the B1 (Co-rich) site spins have a modulated (0.5 k_y 0.5) order with refined $k_y = 0.416(2)$. Powder neutron analysis cannot distinguish between spin density wave (amplitude-modulated) and cycloidal (angle-modulated) spin structures, as reported for $MnVO_3$,[9] and

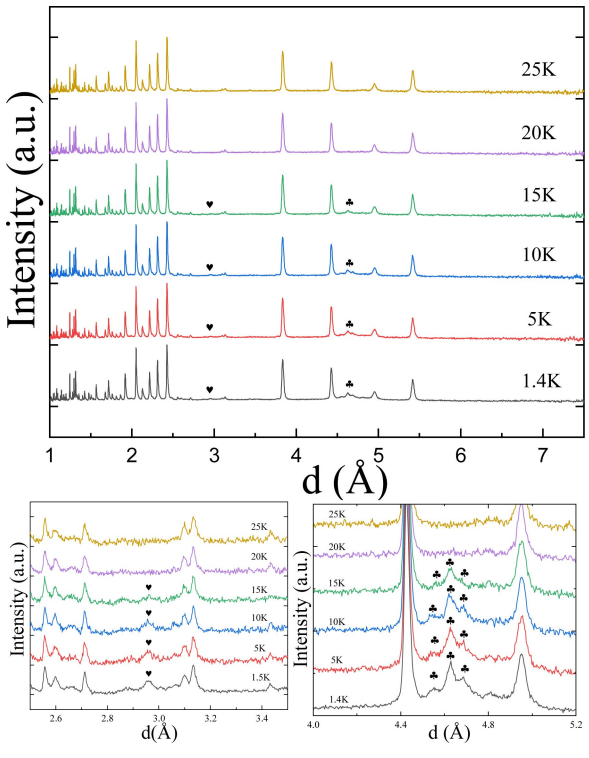

Figure 5. Low temperature powder neutron patterns of $CaMnCoWO_6$ with magnetic peaks marked by symbols and expanded on the lower plots. The envelope at $d = 4.5$–4.7 Å (lower right plot) comprises a central peak from commensurate (0.5 0.5 0.5) order flanked by a pair of satellites from the incommensurate (0.5 0.42 0.5) vector.

we have used the amplitude-modulated model in view of the high anisotropy of Co^{2+}. This model and the profile fit at 1.4 K are shown in Figure 6. All spins lie parallel to the *b*-axis and the moment amplitudes are 1.2(1) μ_B at the A1 and A2 sites, and 2.0(1) μ_B at the B1 sites at 1.4 K.

Fits to the magnetic peaks at 5, 10 and 15 K showed that k_y does not vary with temperature. The two magnetic moments (Fig. 6c) show quite different thermal variations as the B-site moment decreases notably between 10 and 15 K whereas the A-site moment remains almost constant. Although few temperature points are available, it is evident that the ordered A and B site monents have quite different critical exponents. The ordered moments μ were fitted assuming a continuous transition at $T_C = 18$ K using the critical function $\mu = \tanh(Wt^{\beta})/\tanh(W)$, where $t = (T_C - T)/T_C$ and W is a fitting parameter to allow for higher order contributions to the Landau free energy expansion at large t.[29] The A-site spins have critical exponent $\beta = 0.23(3)$ which is within error of the theoretical value of 0.25 for tricritical behavior whereas the B-site spins have $\beta = 0.5(1)$ which indicates mean field behavior (theoretical $\beta = 0.5$). This is of potential interest as it implies a linear-quadratic coupling between B and A site moments. Linear (structural)-quadratic (magnetic) coupling has previously been reported for the magnetoelastic phase transitions in MnO and $Fe_{1-x}O$.[30] Further neutron profiles in the critical region would be needed to determine accurate critical exponents and also to explore whether the two spin orders share a common transition temperature as assumed here or have separate ordering transitions. The saturated moments are greatly reduced from respective ideal spin only values of 5 and 3 μ_B for high spin Mn^{2+} and Co^{2+}, showing that substantial disordered spin components are also present. Field alignment of the disordered components is the likely origin of the magnetic hysteresis loop in Fig. 4b, as the long range spin ordering is purely antiferromagnetic (no weak ferromagnetic components are allowed by symmetry).

Overall the synthesis conditions and structure of $CaMnCoWO_6$ are similar to those for previously reported $P4_2/n$ AA′BB′O_6 double double perovskites, and the A′/B cation disorder and off-stoichiometry ($CaMn_{0.8}Co_{1.2}WO_6$) is very similar to that found in $CaMnCoReO_6$ ($CaMn_{0.7}Co_{1.3}ReO_6$). However, $CaMnCoWO_6$ is notable as the first double double perovskite discovered to have a complex spin order, with both commensurate and incommensurate antiferromagnetic contributions, as analogues including $CaMnCoReO_6$ have simple unfrustrated $\boldsymbol{k} = (0\ 0\ 0)$ ferro- or ferri-magnetic structures, while others are spin glasses. Many metal-oxygen-metal pathways are present so a full analysis of the superexchange network in double double perovskites is not practicable, but two empirical factors appear to be important to the spin order in $CaMnCoWO_6$; cation disorder and the magnetic or non-magnetic nature of the B′ cation. Double double perovskites that have minimal cation disorder, or those that have A′/B disorder but with magnetic B′ = Re^{5+} or Re^{6+} cations, have $\boldsymbol{k} = (0\ 0\ 0)$ spin orders. $CaMnFeTaO_6$, $CaMnFeNbO_6$, and $CaFeFeNbO_6$ have substantial B/B′ cation disorder, because of the relatively small charge difference between B = Fe^{3+} and d^0 B′ = Nb^{5+} or Ta^{5+}, as well

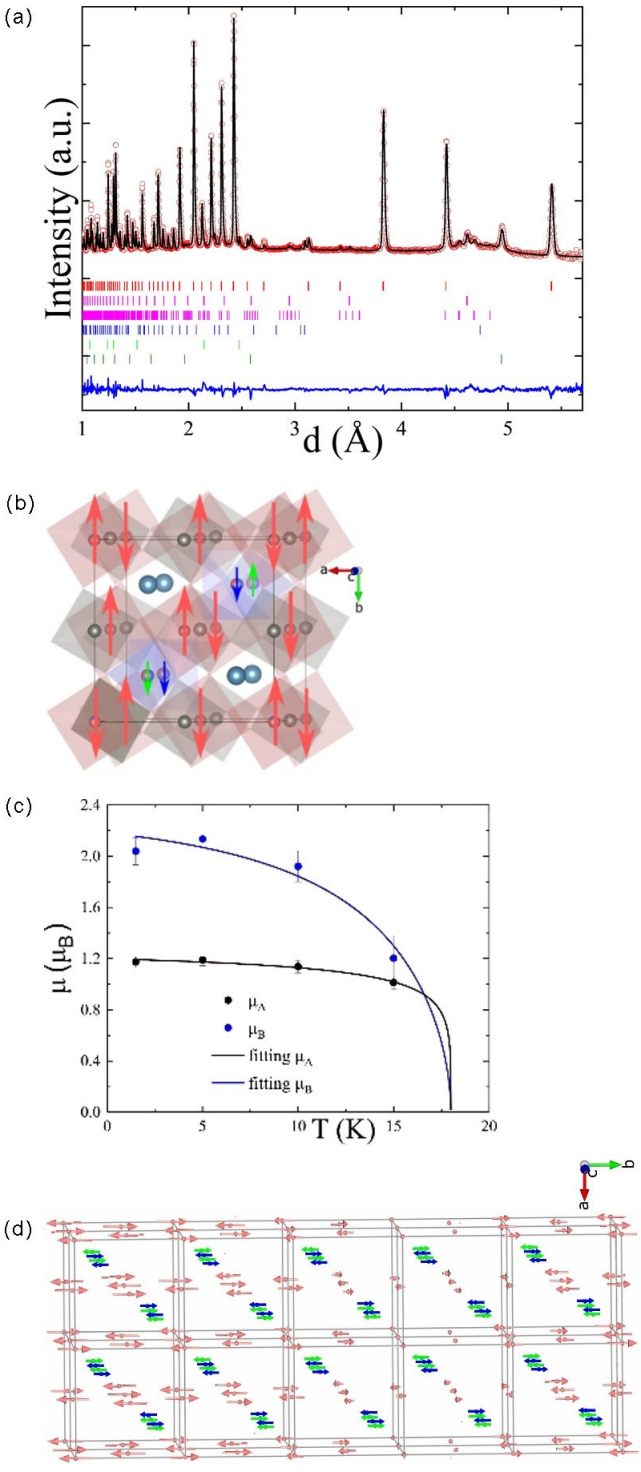

Figure 6. (a) Fit of the crystal and magnetic structure model to the 1.4 K powder neutron diffraction profile. Markers from top to bottom show $CaMnCoWO_6$; crystal structure, (0.5 0.5 0.5) A1,2-sites spin order, (0.5 0.42 0.5) B1-site spin order; $CaWO_4$; (Mn,Co)O nuclear and magnetic contributions. (b) spin order in the crystal unit cell with coordination polyhedra also shown. (c) temperature variations of the A and B site moments with critical fits as described in the text. (d) spin order over 2×5×2 crystal unit cells showing the incommensurate modulation of the B1 spin amplitude. A1/A2/B1 site spins are green/blue/red in (b) and (d).

as A′/B disorder of Mn^{2+} and Fe^{2+} for the former two materials, and are spin glasses. $CaMnCoWO_6$ appears to be intermediate in having A′/B disorder of magnetic Mn^{2+} and Co^{2+} cations, but no B/B′ disorder, and a non-magnetic d^0 B′ = W^{6+} cation. This provides enough frustration to destabilize simple $\boldsymbol{k}$ = (0 0 0) orders, but not enough to fully suppress long range magnetism which would lead to a spin glass. It will thus be interesting to explore further $AA'BB'O_6$ double double perovskites having A′/B disorder of magnetic cations, but with a non-disordered d^0 cation at the B′ site, to discover if other exotic spin orders are stabilized.

Conclusions

Samples of ideal composition $CaMnCoWO_6$, synthesised at high pressure, adopt the tetragonal $P4_2/n$ $AA'BB'O_6$ double double perovskite structure. Co/Mn disorder between A′ and B sites Co^{2+} leads to a Co-rich composition $CaMn_{0.8}Co_{1.2}WO_6$. Both commensurate and incommensurate spin orders (of A′-site spins with propagation vector (0.5 0.5 0.5) and of B-site spins with (0.5 0.42 0.5), respectively) are observed below T_C = 18 K. This is the first observation of complex and incommensurate magnetism in the double double perovskite family and this is attributed to disorder of magnetic Mn^{2+} and Co^{2+} but without disorder of non-magnetic W^{6+}.

Experimental Section

Samples of ideal composition $CaMnCoWO_6$ were prepared using stoichiometric mixtures of $CaWO_4$, CoO and MnO. $CaWO_4$ was prepared by heating a stoichiometric pellet of $CaCO_3$ and WO_3 for 24 hours at 1100 °C. The precursor mixture was packed into a Pt capsule and heated at 1200 °C under 12 GPa pressure in a Walker-type multianvil apparatus. Samples were heated over 10 minutes to the target temperature and held there for 30 minutes before quenching to room temperature, after which the pressure was slowly released.

Laboratory powder X-ray diffraction patterns were collected using a D2 Bruker diffractometer using Cu Kα radiation. Time-of-flight powder neutron diffraction data were measured for 90 min at 1.5 and 150 K and for 30 min at 5, 10, 15, 20, 25, and 50 K at the WISH beamline of the ISIS facility. [31] Rietveld fits were performed using Fullprof software.[32] Data are available at DOI [to be added]. Magnetization was measured using an MPMS SQUID magnetometer.

Acknowledgements

We thank EPSRC for support, and STFC for provision of access to ISIS.

Conflict of Interest

The authors declare no conflict of interest.

Data Availability Statement

Data are available at DOI https://datashare.ed.ac.uk/handle/10283/838.

Keywords: Double double perovskite · incommensurate magnetic structure · powder neutron diffraction · magnetic oxides · high pressure synthesis

[1] R. J. Tilley, *Perovskites: structure-property relationships*, John Wiley & Sons, **2016**.
[2] J. P. Attfield, P. Lightfoot, R. E. Morris, *Dalton Trans.* **2015**, *44*, 10541–10542.
[3] K.-I. Kobayashi, T. Kimura, H. Sawada, K. Terakura, Y. Tokura, *Nature* **1998**, *395*, 677–680.
[4] A. Maignan, B. Raveau, C. Martin, M. Hervieu, *J. Solid State Chem.* **1999**, *144*, 224–227.
[5] D. Serrate, J. De Teresa, M. Ibarra, *J. Phys. Condens. Matter* **2006**, *19*, 023201.
[6] G. King, P. M. Woodward, *J. Mater. Chem.* **2010**, *20*, 5785–5796.
[7] S. Vasala, M. Karppinen, *Prog. Solid State Chem.* **2015**, *43*, 1–36.
[8] E. Solana-Madruga, A. M. Arévalo-López, *J. Solid State Chem.* **2022**, *315* (2022).
[9] M. Markkula, A. M. Arévalo-López, A. Kusmartseva, J. A. Rodgers, C. Ritter, H. Wu, J. P. Attfield, *Phys. Rev. B* **2011**, *84*, 094450.
[10] E. Solana-Madruga, A. J. Dos santos-García, A. M. Arévalo-López, D. Ávila-Brande, C. Ritter, J. P. Attfield, R. Sáez-Puche, *Dalton Trans.* **2015**, *44*, 20441–20448.
[11] A. J. Dos santos-García, E. Solana-Madruga, C. Ritter, D. Ávila-Brande, O. Fabelo, R. Sáez-Puche, *Dalton Trans.* **2015**, *44*, 10665–10667.
[12] A. J. Dos Santos-García, C. Ritter, E. Solana-Madruga, R. Sáez-Puche *J. Phys. Condens. Matter* **2013**, *25*, 206004.
[13] A. M. Arévalo-López, F. Stegemann, J. P. Attfield, *Chem. Commun.* **2016**, *52*, 5558.
[14] A. M. Arevalo-Lopez, G. M. McNally, J. P. Attfield, *Angew. Chem. Int. Ed.* **2015**, *54*, 12074.
[15] M.-R. Li, M. Retuerto, Z. Deng, P. W. Stephens, M. Croft, Q. Huang, H. Wu, X. Deng, G. Kotliar, J. Sanchez-Benitez, J. Hadermann, D. Walker, M. Greenblatt, *Angew. Chem. Int. Ed.* **2015**, *54*, 12069.
[16] C. E. Frank, E. E. McCabe, F. Orlandi, P. Manuel, X. Tan, Z. Deng, M. Croft, V. Cascos, T. Emge, H. L. Feng, S. Lapidus, C. Jin, M. X. Wu, M. R. Li, S. Ehrlich, S. Khalid, N. Quackenbush, S. Yu, D. Walker, M. Greenblatt, *Chem. Commun.* **2019**, *55*, 3331–3334.
[17] E. Solana-Madruga, K. N. Alharbi, M. Herz, P. Manuel, J. P. Attfield, *Chem. Commun.* **2020**, *56*, 12574–12577.
[18] E. Solana-Madruga, Á. M. Arévalo-López, A. J. Dos Santos-García, E. Urones-Garrote, D. Ávila-Brande, R. Sáez-Puche, J. P. Attfield, *Angew. Chem. Int. Ed.* **2016**, *55*, 9340–9344.
[19] E. Solana-Madruga, Á. M. Arévalo-López, A. J. Dos santos-García, C. Ritter, C. Cascales, R. Sáez-Puche, J. P. Attfield, *Phys. Rev. B* **2018**, *97*, 134408.
[20] K. Ji, Y. Yuan, G. T. Moy, C. Ritter, J. P. Attfield, *J. Solid State Chem.* **2022**, *313*, 123329.
[21] G. M. McNally, Á. M. Arévalo-López, P. Kearins, F. Orlandi, P. Manuel, J. P. Attfield, *Chem. Mater.* **2017**, *29*, 8870–8874.
[22] G. M. McNally, A. M. Arévalo-López, F. Guillou, P. Manuel, J. P. Attfield, *Phys. Rev. Mater.* **2020**, *4*, 064408.
[23] E. Solana-Madruga, Y. Sun, Á. M. Arévalo-López, J. P. Attfield, *Chem. Commun.* **2019**, *55*, 2605–2608.

[24] P. Kearins, E. Solana-Madruga, K. Ji, C. Ritter, J. P. Attfield, *J. Phys. Chem. C* **2021**, *125*, 9550–9555.
[25] E. Solana-Madruga, P. S. Kearins, K. N. Alharbi, C. T. Lennon, C. Ritter, J. P. Attfield, *Phys. Rev. Mater.* **2021**, *5*, 054412.
[26] K. Ji, K. N. Alharbi, E. Solana-Madruga, G. T. Moyo, C. Ritter, J. P. Attfield, *Angew. Chem. Int. Ed.* **2021**, *133*, 22422.
[27] K. Ji, J. R. Bedward, Q. Li, P. Manuel, C. Ritter, J. P. Attfield, *Chem. Commun.* **2023**, *59*, 6371–6374.
[28] E. Solana-Madruga, P. S. Kearins, C. Ritter, A. M. Arévalo-López, J. P. Attfield, *Angew. Chem. Int. Ed.* **2022**, *61*, e202209497.
[29] M. S. Senn, J. P. Wright, J. Cumby, J. P. Attfield, *Phys. Rev. B* **2015**, *92*, 024104.
[30] M. A. Carpenter, Z. Zhang, C. J. Howard, *J. Phys. Condens. Matter* **2012**, *24*, 156002.
[31] L. C. Chapon, P. Manuel, P. G. Radaelli, C. Benson, L. Perrott, S. Ansell, N. J. Rhodes, D. Raspino, D. Duxbury, E. Spill, J. Norris, *Neutron News* **2011**, *22*, 22–25.
[32] J. Rodriguez-Carvajal, *Physica B + C* **1993**, *192*, 55–69.

Manuscript received: March 23, 2023
Revised manuscript received: June 7, 2023
Accepted manuscript online: June 14, 2023

RESEARCH ARTICLE

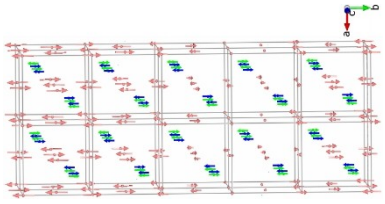

*Dr. K. Ji, R. Chen, Dr. P. Manuel, Prof. J. P. Attfield**